Electron interaction with confined acoustic phonons in quantum wires subjected to a magnetic field

A. Svizhenko, A. Balandin, and S. Bandyopadhyay
Department of Electrical Engineering, University of Nebraska, Lincoln, Nebraska 68588

M. A. Stroscio
U.S. Army Research Office, P.O. Box 12211, Research Triangle Park, North Carolina 27709
(Received 17 July 1997)

We have studied the effect of an external magnetic field on electron-acoustic phonon scattering in rectangular quantum wires taking into account both electron and phonon confinement. A magnetic field has two major effects: (i) it dramatically quenches (by several orders of magnitude) intrasubband scattering due to acoustic phonons in hybrid ''width'' and ''thickness'' modes, and (ii) it increases electron interaction with evanescent hybrid surface modes that peak at the wire edges. A simple intuitive picture to elucidate the origin of these effects is presented.
[S0163-1829(98)08908-5]

I. INTRODUCTION

Electron-phonon interaction in quantum wires has been studied by a number of researchers in the past.[1–13] References 4–10 studied the effect of an external magnetic field on electron scattering rates assuming bulk (unconfined) acoustic phonons, while Refs. 11–13 accounted for the confined nature of acoustic phonons but omitted any effects of a magnetic field. In this paper, we report the first study of electron-phonon interaction taking into account both the effects of an external magnetic field and phonon confinement.

Phonon confinement is expected to be important whenever the transverse dimensions of a quantum wire are smaller than the phonon coherence length. It increases electron-phonon scattering rates by several orders of magnitude,[11–13] and in the presence of a magnetic field, it assumes an added importance. The scattering rate depends primarily on two quantities; the joint electron-phonon density of states, and the interaction matrix element, which is determined by the overlap between three scalars: the wave function of the electron's initial state, the wave function of the final state, and the phonon's normal mode. Both quantities are influenced strongly by a magnetic field when phonon confinement effects are present. First, confinement causes significant nonlinearities in the dispersion relations of acoustic-phonon modes and modifies the phonon density of states. The electron density of states (in magnetoelectric subbands) is also strongly influenced by the magnetic field.[14] As a result, the joint density of electron-phonon states, which determines the scattering rate, can be modulated by the magnetic field. Second, and perhaps more importantly, a magnetic field skews the wave functions of a traveling electron state towards one edge of the wire (''edge states''). This significantly alters the overlap between the electron's initial and final states' wave function and the phonon mode. Obviously, the overlap with surface phonon modes is increased and this increases the surface phonon mediated scattering. Additionally, the wave function of an electron in the mth subband is no longer orthogonal to the nth phonon mode for $m \neq n$. As a result many new scattering channels are opened corresponding to $m \neq n$, which were previously forbidden. Third, and most important, there is an effect that strongly influences electron-phonon scattering in relatively wide wires. If the wire width is much larger than the magnetic length $\sqrt{\hbar/qB}$ (q is electronic charge and B is the magnetic flux density), then oppositely traveling electron states in a quantum wire are skewed towards opposite edges of the wire by a magnetic field. As a result, the overlap between their wave functions decreases and the probability of ''backscattering'' (scattering between oppositely traveling states) is reduced. This was predicted before[6] in the context of electron interaction with bulk acoustic modes. We found that intrasubband backscattering rates can be suppressed by four orders of magnitude in GaAs wires with widths ~ 400 Å at a magnetic flux density of 10 T. Since backscattering is usually the dominant interaction with acoustic phonons, its suppression decreases the total electron-phonon scattering rate at low temperatures. This is an important result since the quenching of backscattering in a magnetic field is an important ingredient in the Büttiker picture of the integral quantum Hall effect.[15]

The paper is organized as follows. In the next section we describe the calculation of electron eigenstates in a quantum wire subjected to an external magnetic field. We compute the wave functions, the dispersion relations and the density of states (at a given energy) in various magnetoelectric subbands. This is an exact and rigorous treatment. In Sec. III, we derive the acoustic-phonon eigenmodes in a quantum wire assuming that a magnetic field does not affect phonons. The normal modes of acoustic phonons are dilatational (or compressional), flexural, torsional and shear.[13] These modes have been calculated recently[13] using a so-called xyz algorithm.[16] To simplify the calculation, we have employed Morse's ansatz,[17,18] which allows us to combine approximately all these modes into two hybrid modes: ''width'' modes and ''thickness'' modes corresponding to the width and the thickness of the quantum wire (these are not true ''normal modes'' of the system, however). Even though this approach

 © 1998 The American Physical Society

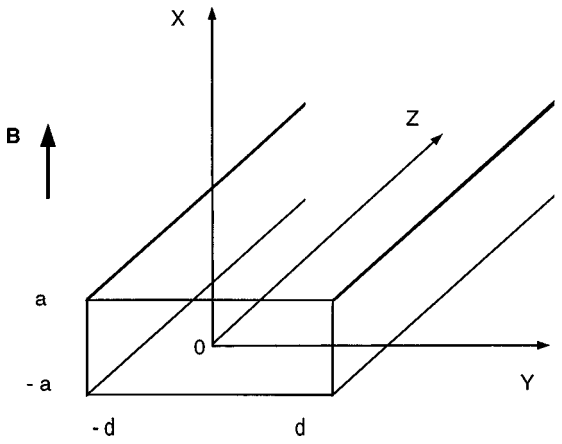

FIG. 1. A rectangular electron waveguide (quantum wire) subjected to a magnetic field along x axis. The width of the wire is much larger than the thickness.

misses the edge modes of Ref. 13, it is not a serious deficiency since edge modes are not very important for electron-phonon interaction. Since the electron wave function always decays at the edges of the quantum wire, the matrix element for electron interaction with edge phonon modes is negligibly small. We point out that in spite of using Morse's ansatz, which was used by Refs. 11 and 12, we have found many new branches in the phonon spectra that Refs. 11 and 12 missed because they assumed particular forms of the solutions for the lattice displacements. We make no *a priori* assumption about the forms and solve the secular equations for the displacements exactly. This reveals the existence of new branches in the dispersion relations. Finally, in Sec. IV, we consider electron-phonon interaction in a magnetic field and calculate the relevant scattering rates. Conclusions are presented in Sec. V.

II. ELECTRON EIGENSTATES IN MAGNETOELECTRONIC SUBBANDS

We consider a quantum wire as shown in Fig. 1 with a constant magnetic field directed along the x direction. The thickness along this x direction is so small that only the lowest transverse subband in this direction will be occupied under all circumstances. This restriction, coupled with the fact that the x-directed magnetic field does not affect the x component of the electron wave function, allows us to drop the x component from further consideration (we assume that the x component of the electron wave function is always the lowest particle-in-a-box state). The time-independent Schrödinger equation describing our system is given by

$$\frac{[(\mathbf{p}-e\mathbf{A})]^2}{2m^*}\psi(z,y)+V(y)\psi(z,y)=E\psi(z,y), \qquad (1)$$

where $V(y)$ is the confining potential in the y direction and $\mathbf{A}$ is the magnetic vector potential. We neglect spin effects and assume hard-wall boundary conditions on $V(y)$. For a Landau gauge

$$\mathbf{A}=(0,0,-By), \qquad (2)$$

where B is the magnetic flux density, the solution for the wave function is

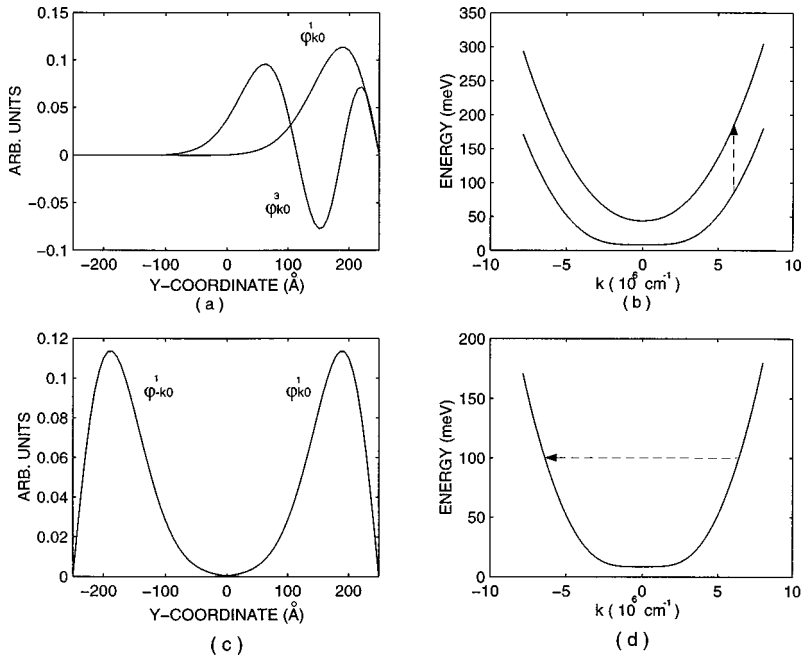

FIG. 2. Electron wave functions and dispersion relations in a GaAs quantum wire subjected to a magnetic field of 10 T. (a) Wave functions of electrons in the first and the third subbands with wave vector $k_z=7\times10^6$ cm^{-1} skewed by a magnetic field. (b) Dispersion relations for the first and the third subbands. (c) Wave functions of oppositely moving electrons in the first subband with $k_z=\pm7\times10^6$ cm^{-1}. (d) Dispersion relation for the first subband and schematic elastic scattering process between two states.

$$\psi(z,y)=e^{ik_z z}\phi_\nu(y), \tag{3}$$

where k_z is the electron wave vector along the wire's length, and $\phi_\nu(y)$ is the y component of the wave function for the state with wave vector k_z in the νth magnetoelectric subband. It obeys the equation

$$\frac{\partial^2\phi(y)}{\partial y^2}+\frac{2m^*}{\hbar^2}E\phi(y)-\left(\frac{y}{l^2}\right)^2\phi(y)$$

$$+2\frac{y}{l^2}k\phi(y)-k^2\phi(y)=0 \tag{4}$$

with boundary conditions

$$\phi(-d)=\phi(d)=0. \tag{5}$$

Here l is the magnetic length. This equation is solved numerically following the prescription of Ref. 14 to yield the wave functions, energy dispersion relations, and density of states in hybrid magnetoelectric subbands. Some examples are shown in Fig. 2.

III. CONFINED ACOUSTIC PHONON EIGENMODES

The derivation of confined acoustic phonon eigenmode was reported in Refs. 11–13, 17, and 18. In this paper we employ the approximate technique of Refs. 11, 12, 17 and 18, but unlike them, do not assume *a priori* any particular form of the solutions for the ionic displacements.

The elasticity equation can be written as[11,12,17,18]

$$\frac{\partial^2\mathbf{u}}{\partial t^2}=s_t^2\boldsymbol{\nabla}^2\mathbf{u}+(s_l^2-sd_t^2)\boldsymbol{\nabla}(\boldsymbol{\nabla}\cdot\mathbf{u}), \tag{6}$$

where $\mathbf{u}$ is the displacement vector, and s_l and s_t are the speeds of longitudinal and transverse acoustic waves in bulk media. For GaAs, $s_l=4.78\times10^5$ cm/s and $s_t=3.35\times10^5$ cm/s in the [001] direction.

We assume that the width of the wire is $2d$ and the thickness is $2a$. The origin of the coordinates is located at the geometric center of the cross section. The normal components of the stress tensors on free-standing surfaces must vanish; consequently, the boundary conditions for free standing quantum wires are $\sigma_{x,x}=\sigma_{y,x}=\sigma_{z,x}=0$ at $x=\pm a$ and $\sigma_{x,y}=\sigma_{y,y}=\sigma_{z,y}=0$ at $y=\pm d$. To find the eigenmodes for acoustic vibrations defined by Eqs. (6), we follow Morse's assumption of separation of variables,[17,18] which allows us to decompose the modes into ''thickness'' modes and ''width'' modes. For the former, the solutions can be expressed in the form

$$\mathbf{u}_\mathbf{x}^\mathbf{t}=A_t u_t(\gamma,x)\cos(hy)e^{i\gamma(z-ct)}, \tag{7}$$

$$\mathbf{u}_\mathbf{y}^\mathbf{t}=A_t v_t(\gamma,x)\sin(hy)e^{ixg(z-ct)}, \tag{8}$$

$$\mathbf{u}_\mathbf{z}^\mathbf{t}=A_t w_t(\gamma,x)\cos(hy)e^{i\gamma(z-ct)}, \tag{9}$$

where γ is the z-directed longitudinal-phonon wave vector along the length of the wire, c is the phase velocity of sound, and $h=(n+1/2)\pi/d$ (n is an integer). We will choose only the principal mode corresponding to $n=0$ based on Morse's experimental observation that this mode is dominant.[17] Accordingly, $h=\pi/2d$. For ''width'' modes, the displacements are

$$\mathbf{u}_\mathbf{x}^\mathbf{w}=A_w u_w(\gamma,y)\sin(\kappa x)e^{i\gamma(z-ct)}, \tag{10}$$

$$\mathbf{u}_\mathbf{y}^\mathbf{w}=A_w v_w(\gamma,y)\cos(\kappa x)e^{i\gamma(z-ct)}, \tag{11}$$

$$\mathbf{u}_\mathbf{z}^\mathbf{w}=A_w w_w(\gamma,y)\cos(\kappa x)e^{i\gamma(z-ct)} \tag{12}$$

with $\kappa=0$ for the principal modes. To complete the solutions, we need to find $u_t(\gamma,x)$, $u_w(\gamma,y)$, $v_t(\gamma,x)$, $v_w(\gamma,y)$, $w_t(\gamma,x)$, and $w_w(\gamma,y)$. These are found from the secular equations

$$D_t\begin{pmatrix}u_t(\gamma,x)\\ v_t(\gamma,x)\\ w_t(\gamma,x)\end{pmatrix}=-\omega_n^2\begin{pmatrix}u_t(\gamma,x)\\ v_t(\gamma,x)\\ w_t(\gamma,x)\end{pmatrix}, \tag{13}$$

$$\frac{\partial u_t}{\partial x}=0,\quad \frac{\partial v_t}{\partial x}=hu_t,\quad \frac{\partial w_t}{\partial x}=-i\gamma u_t, \tag{14}$$

and

$$D_w\begin{pmatrix}v_w(\gamma,y)\\ w_w(\gamma,y)\end{pmatrix}=-\omega_n^2\begin{pmatrix}v_w(\gamma,y)\\ w_w(\gamma,y)\end{pmatrix}, \tag{15}$$

$$\frac{\partial v_w}{\partial y}=0,\quad \frac{\partial w_w}{\partial y}=-i\gamma v_w \tag{16}$$

for thickness and width modes, respectively. Here ω_n is the angular frequency of the nth phonon branch for a phonon longitudinal wave vector γ. The differential matrix operators are given by

$$D_t=\begin{pmatrix}s_l^2\partial_{xx}-s_t^2(h^2+\gamma^2) & h(s_l^2-s_t^2)\partial_x & i\gamma(s_l^2-s_t^2)\partial_x\\ -h(s_l^2-s_t^2)\partial_x & s_t^2\partial_{xx}-s_t^2\gamma^2-s_l^2h^2 & -i\gamma h(s_l^2-s_t^2)\\ i\gamma(s_l^2-s_t^2)\partial_x & i\gamma h(s_l^2-s_t^2) & s_t^2\partial_{xx}-s_t^2h^2-s_l^2\gamma^2\end{pmatrix} \tag{17}$$

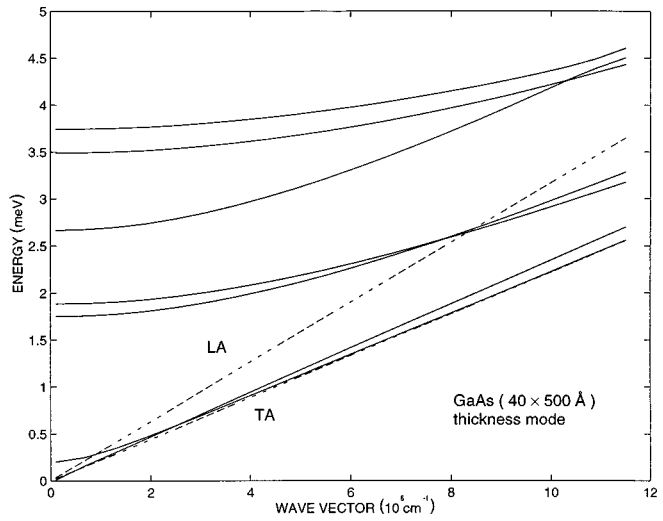

(a)

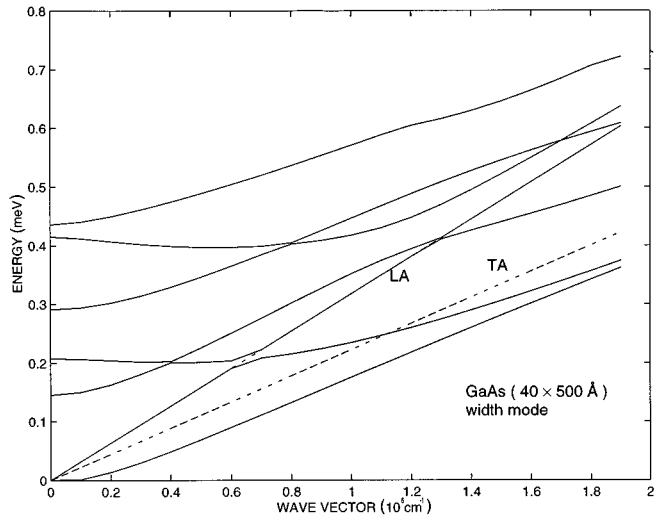

(b)

FIG. 3. Dispersion relations for the seven lowest width (a) and thickness (b) modes of a 40×500 Å GaAs quantum wire. The dashed lines are the dispersion curves of the bulk LA and TA waves along the [001] direction. Branches that are below the LA curve correspond to surface waves.

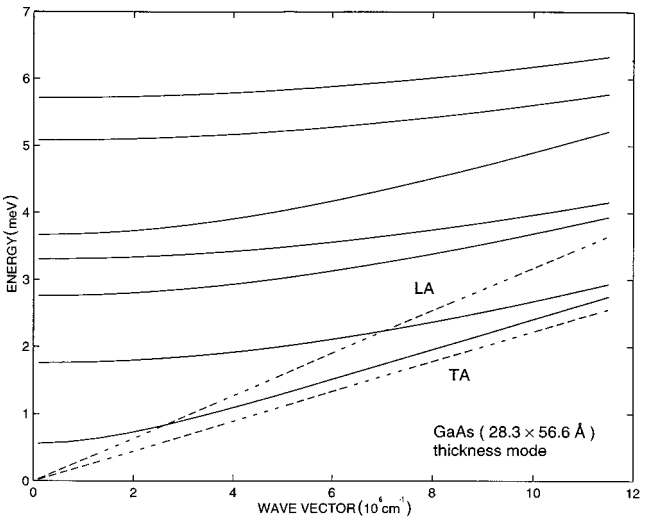

(a)

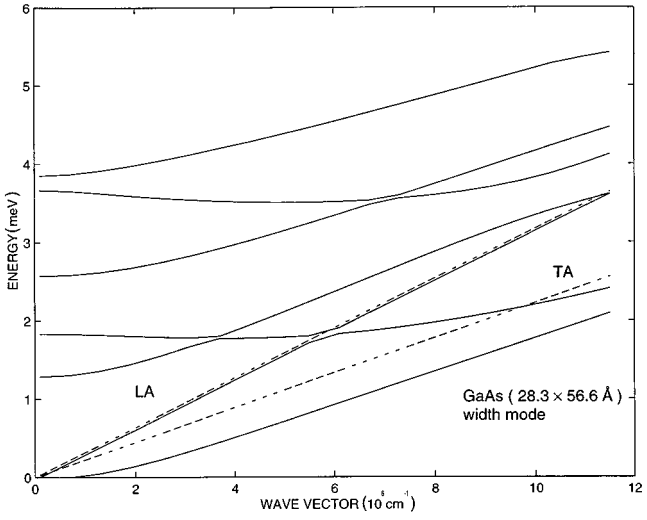

(b)

FIG. 4. Dispersion relations for the seven lowest width (a) and thickness (b) modes of a 28.3×56.6 Å GaAs quantum wire. The dashed lines are the dispersion curves of the bulk LA and TA waves along the [001] direction. Again, branches below the LA curve correspond to surface waves.

and

$$D_w = \begin{pmatrix} s_l^2\partial_{yy} - s_t^2\gamma^2 & i\gamma(s_l^2 - s_t^2)\partial_y \\ i\gamma(s_l^2 - s_t^2)\partial_y & s_t^2\partial_{yy} - s_l^2\gamma^2 \end{pmatrix}. \tag{18}$$

We make no further assumptions about the form of displacements and solve the one-dimensional eigenvalue problems (13) and (14) and (15) and (16) exactly, using the numerical finite difference scheme. The solutions yield the dispersion relations ω_n versus γ for the 1...n phonon modes. In Fig. 3(a) and 3(b), we show the dispersion relations of thickness and width modes for a GaAs quantum wire with width=500 Å and thickness=40 Å. The dashed straight lines are the dispersion relations for bulk longitudinal and transverse acoustic phonons. In Figs. 4(a) and 4(b) we also show the dispersion relations for a quantum wire with cross-sectional dimensions 28.3×56.6 Å for comparison with Refs. 11 and 12, which used these dimensions. The comparison reveals many new branches that were not found in Refs. 11 and 12. They were obviously lost when certain forms were assumed in Refs. 11 and 12 for the solutions of $u_t(\gamma,x)$, $u_w(\gamma,y)$, $v_t(\gamma,x)$, $v_w(\gamma,y)$, $w_t(\gamma,x)$, and $w_w(\gamma,y)$. One should note that $u_t(\gamma,x)$, $u_w(\gamma,y)$, $v_t(\gamma,x)$, $v_w(\gamma,y)$, $w_t(\gamma,x)$, and $w_w(y)$ combine the characters of the normal modes: dilatational (compressional), flexural, torsional, and shear. That is why the thickness and width modes are hybrid modes and not true normal modes of the system.

Finally, the amplitudes A_t and A_w for thickness and width modes are found from the energy quantization condition:

$$\frac{A^2}{4ad}\int_{-a}^{+a}dx\int_{-d}^{+d}dy[uu^*+vv^*+ww^*]=\frac{\hbar}{2M\omega_\gamma}, \tag{19}$$

where ω_γ is the radial frequency of the mode with wave vector γ and M is the mass of an ion.

An important insight can be gained from the generic wave-vector relations,

$$k_d^2+h^2+\gamma^2=(\omega/c_d)^2,$$

$$k_s^2+h^2+\gamma^2=(\omega/c_s)^2, \tag{20}$$

where $k_{d,s}$ is the transverse wave-vector component of dilational (longitudinal) and shear waves, respectively. They are related to the Lamé constants λ' and μ as

$$c_d^2=(\lambda'+2\mu)/\rho, \tag{21}$$

$$c_s^2=\mu/\rho, \tag{22}$$

where ρ is the mass density.

If a branch in the phonon spectra (see Figs. 3 and 4), or a portion thereof, falls below the longitudinal-acoustic (LA) branch (the slope of which is c_d), then k_d becomes imaginary for that branch. This is an evanescent mode that is localized near the edges of the wire and is termed a ''surface mode.'' Similarly, if a branch falls below the transverse-acoustic (TA) branch, k_s is imaginary and it is also an evanescent surface mode.

IV. CONFINED ELECTRON-CONFINED ACOUSTIC-PHONON INTERACTION AND SCATTERING RATES IN A MAGNETIC FIELD

The deformation-potential interaction of an electron with an acoustic phonon at a certain wave vector γ is described by the Hamiltonian $H_{\rm def}(\gamma)$ given by[11,12]

$$H_{\rm def}(\gamma)=E_a\nabla\cdot\mathbf{u}(\mathbf{r})$$

$$=E_a\sum_{n,m}[c_{n,m}(\gamma)+c_{n,m}^+(-\gamma)]$$

$$\times\left[\frac{\partial u}{\partial x}+\frac{\partial v}{\partial y}+i\gamma w\right]e^{i\gamma z}, \tag{23}$$

where $c_{n,m}(\gamma)$ and $c_{n,m}^+(-\gamma)$ are annihilation and creation operators and

$$\mathbf{u}(\mathbf{r})=\sum_{\gamma,n,m}[c_{n,m}(\gamma)+c_{n,m}^+(-\gamma)]\mathbf{u}(x,y,\gamma)e^{i\gamma z}. \tag{24}$$

The summation is taken over all acoustic-phonon modes. The Fermi golden rule scattering rate for an electron scattering from an energy state E_ν in subband ν to an energy state $E'_{\nu'}$ is subband ν' by absorbing or emitting a phonon of longitudinal wave vector γ and energy ω_γ is given by

$$S(E_\nu,E'_{\nu'},\pm\gamma,\pm\omega_\gamma)=\frac{2\pi}{\hbar}|M(E_\nu,E'_{\nu'})|^2(N+1/2\mp1/2)$$

$$\times\delta(E_\nu-E'_{\nu'}\pm\hbar\omega_\gamma)\delta_{k'-k,\pm\gamma}, \tag{25}$$

where the upper sign refers to absorption and the lower to emission. The first δ function represents the usual energy conservation and the second Krönicker δ represents momentum conservation along the wire axis. Here, k and k' are the initial and final wave vectors of the electron along the wire axis, N is the Bose-Einstein occupation number for acoustic phonons, and $M(E_\nu,E'_{\nu'})$ is the matrix element of Hamiltonian (23) taken between electron envelope wave functions $\sqrt{1/a}\,\phi(y,k_z^0)\cos(\pi x/2a)$ and $\sqrt{1/a}\,\phi(y,k_z^0\pm\gamma)\cos(\pi x/2a)$ of initial and final states:

$$M(E_\nu,E'_{\nu'})=E_a\cdot\begin{cases}\frac{1}{a}<\cos(\frac{\pi x}{2a})|\frac{\partial u}{\partial x}+\frac{\pi}{2d}v+i\gamma w|\cos(\frac{\pi x}{2a})>\times\\ <\phi^*(y,E'_{\nu'})|\cos(\frac{\pi y}{2d})|\phi(y,E_\nu)>,\\ \text{for thickness mode}\\ \\ <\phi^*(y,E'_{\nu'})|\frac{\partial v}{\partial y}+i\gamma w|\phi(y,E_\nu)>,\\ \text{for width mode}\end{cases} \tag{26}$$

Depending on the sign of γ and $\hbar\omega_\gamma$ we distinguish among four types of scattering: forward and backward absorption and forward and backward emission. In forward scattering, the electron momentum increases, while in backward scattering it decreases. Typically, in backward scattering, the direction of an electron's motion will be turned around. Therefore, this will involve scattering between initial and final states that have opposite directions of motion. Since a magnetic field spatially separates these two states by localizing them along opposite edges of a wire [see Fig. 2(c)], the matrix element for backscattering will be dramatically reduced. This can be clearly seen from Eq. (26) in the case of thickness modes.

For each type of scattering, the total scattering rate for an electron initially at an energy E in the νth magnetoelectric subband can be obtained by integrating over all possible final

states and phonon wave vectors,

$$S(E_\nu)=\int_0^\infty\int_0^{\gamma_{\max}} dE'_{\nu'}\,d\gamma\,S(E_\nu,E'_{\nu'},\pm\gamma,\pm\omega_\gamma)$$

$$=\frac{1}{\hbar}\sum_{E_\nu-E'_{\nu'}\pm\hbar\omega_\gamma=0} D(E'_{\nu'},\omega_\gamma)|M(E_\nu,E'_{\nu'})|^2$$

$$\times(N+1/2\mp1/2), \tag{27}$$

where $D(E'_{\nu'},\omega_\gamma)$ is the joint electron-phonon density of states and $\gamma_{\max}$ is the maximum phonon wave vector (which will be the Debye wave vector if we neglect Umklapp processes). In the equation above, we changed the double integration over all possible final states and the energy conserving δ function by the summation over all zeros of the function $f=E_\nu-E'_{\nu'}\pm\hbar\omega_\gamma$. Its inverse derivative $D(E'_{\nu'},\omega_\gamma)$ plays the role of the one-dimensional joint electron-phonon density of states, which is defined as

$$D(E'_{\nu'},\omega_\gamma)=\sum_n \frac{2\pi}{\partial(E_\nu-E'_{\nu'}\pm\hbar\omega_\gamma)/\partial\gamma}$$

$$\times\theta(E_\nu-E'_{\nu'}\pm\hbar\omega_\gamma), \tag{28}$$

where θ is the Heaviside (unit step) function and n is the number of phonon branches at a frequency ω_γ. Therefore, the behavior of the scattering rate reflects the features of both the electron and phonon densities of states.

The same procedure can be applied for polar acoustic phonons (piezo-electric scattering). The piezoelectric-potential interaction[19] depends on the displacement along wire axis only and is described by

$$H_{\rm PZ}=\frac{qe_{\rm PZ}}{\epsilon\epsilon_0}\sum_{\gamma,n,m}[c_{n,m}(\gamma)+c^+_{n,m}(-\gamma)]w(x,y,\gamma)e^{i\gamma z}, \tag{29}$$

where $e_{\rm PZ}$ is the piezoelectric constant and for GaAs, it is 0.16 C/m^2 along the [100] axis.

V. RESULTS AND CONCLUSION

In Figs. 5 and 6, we plot the total scattering rate (intrasubband plus intersubband)—associated with deformation potential and piezoelectric interactions—versus electron energy. All scattering rates are calculated for GaAs wires with the z axis along the [100] direction and at a lattice temperature of 77 K. In other words, we are plotting the quantity $1/\tau(E)=\Sigma_\nu S(E_\nu)$ versus E after summing over all subbands at energy E. These rates are plotted for two cases: there is no magnetic field, and a magnetic flux density of 10 T is present. Two features stand out. First, in Fig. 5(a), the energy dependence of the scattering rates is fairly constant if we neglect the fine structures associated with peaks and valleys in the joint density of electron-phonon states. However, when a magnetic field of 10 T is turned on, we can easily resolve the scattering rates associated with intrasubband transitions within the lowest magnetoelectric subband and the intersubband transitions to the next higher subband, which becomes accessible in energy past 25 meV. As expected, the intrasubband transition rate decrease monotonically with energy because the joint density of states has this dependence

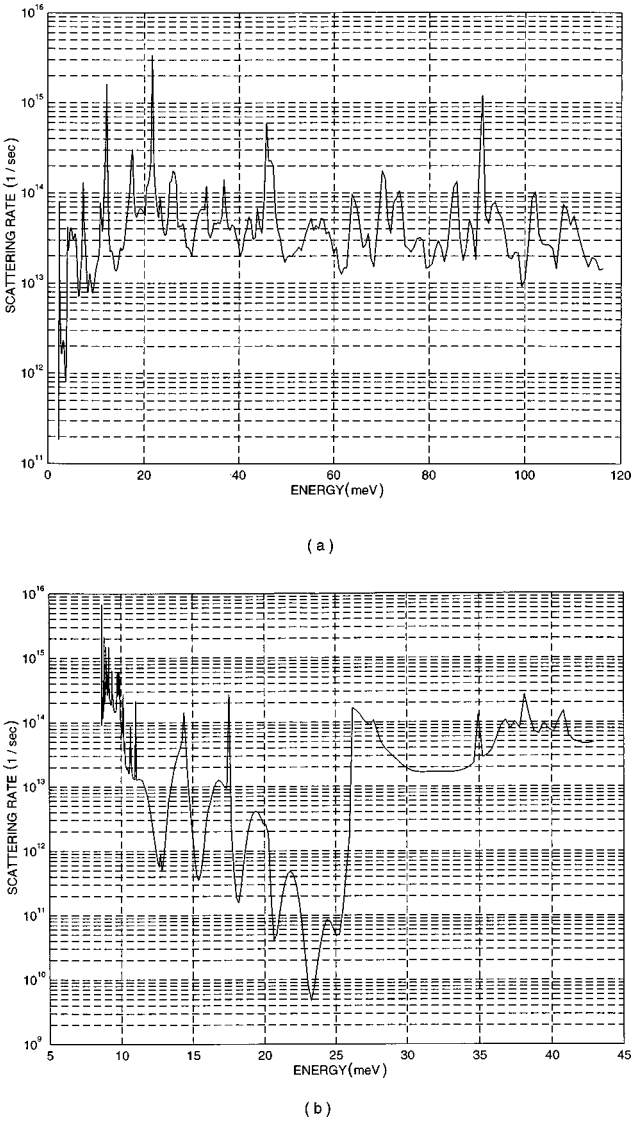

FIG. 5. Scattering rates vs energy for deformation-potential-interaction in a 40×500 Å GaAs quantum wire at magnetic field (a) 0 T and (b) 10 T. Energy is measured from the bulk conduction band edge. The lattice temperature is 77 K.

within any magnetoelectric subband. This resolution between subbands is lost without a magnetic field because the subband spacing is too small for a 500 Å wire. In Fig. 5(b), as soon as the second subband becomes accessible in energy, the scattering rate increases rapidly and shows a divergence associated with the singularity in the density of states at the second subband bottom. Comparing Figs. 5(a) and 5(b), one can see that the magnetic field decreases the scattering rate by *four orders of magnitude* just before the second subband becomes accessible. It happens because of the previously mentioned suppression of backscattering in a magnetic field. This suppression becomes progressively larger at higher energies within a subband because of the following reason. The spatial separation between the wave functions of oppositely travelling states—which is responsible for the quenching of backscattering—can be viewed as being caused by the Lorentz force pushing oppositely traveling electrons in opposite directions. Since the Lorentz force is proportional to the electron velocity, the degree of spatial separation the wave

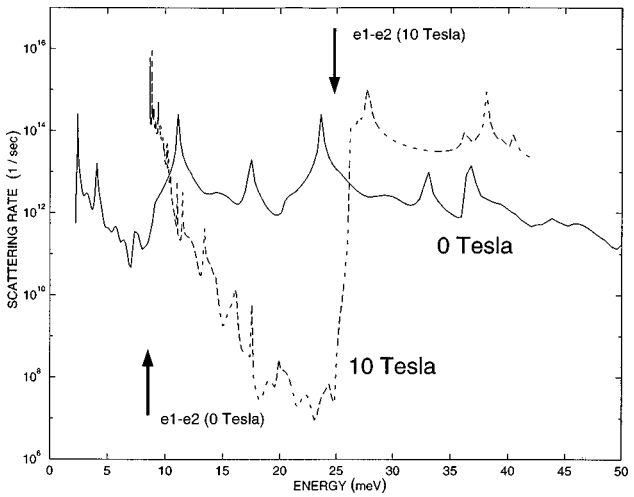

FIG. 6. Scattering rates vs energy dependence for piezoelectric-potential interaction in a 40×500 Å GaAs quantum wire at magnetic field 0 and 10 T. The lattice temperature is 77 K.

functions and the degree of suppression of backscattering will increase at higher electron energies. That is why the degree of ''quenching'' increases with increasing energy within any subband.

The same magnetic-field-induced quenching is evident in the case of piezoelectric scattering the rates of which are plotted in Fig. 6. Here one should note that the scattering rate at energies above the second subband bottom actually increases slightly when a magnetic field is applied. It happens because this rate is dominated by intersubband scattering from the first subband to the second subband. Unlike in the case of intrasubband scattering, backscattering is *not* the dominant mechanism for *intersubband* scattering. Consequently, the other two effects that we mentioned in Sec. I play a significant role. These are (i) the opening of new scattering channels (electrons in the nth subband along the width interacting with phonons in the mth width mode even when $m\neq n$) and (ii) the increased interaction with surface phonons when the electron wave functions are skewed by the magnetic field towards the edges of the wire. Both of these effects tend to increase the scattering rate and this is what we observe in Fig. 6 past an energy of 25 meV.

In conclusion, we have calculated the scattering rates of confined electrons with confined acoustic phonons in a quantum wire subjected to a magnetic field. We find that a magnetic field can drastically quench intrasubband scattering. Obviously, this has an important bearing on the Buttiker picture of the integral quantum Hall effect, which invokes the suppression of backscattering between edge states in a Hall bar to explain the vanishing of longitudinal resistance and the quantization of the Hall resistance. Furthermore, it will result in strong negative magnetoresistance in quantum wires whenever acoustic phonon interactions determine the resistance (namely, at low temperatures). Unexplained negative magnetoresistance has recently been observed in experiments with GaAs quantum wells (the same phenomenon can be observed in both wires and wells) which could not be ascribed to weak localization effects.[20] These and other related phenomena[21] may be associated with suppression of acoustic-phonon scattering. Finally, such effects can find applications in magnetic-field sensors and they can be used to enhance the mobility of electrons in quantum wires.

ACKNOWLEDGMENT

This work was supported by the U.S. Army Research Office.

[1] S. Briggs and J. P. Leburton, Phys. Rev. B **38**, 8163 (1988).
[2] D. Jovanovic, S. Briggs and J. P. Leburton, Phys. Rev. B **42**, 11 108 (1990).
[3] K. W. Kim, M. A. Stroscio, A. Bhatt, R. Mickevicius, and V. V. Mitin, J. Appl. Phys. **70**, 319 (1991).
[4] N. Mori, H. Momose, and C. Hamaguchi, Phys. Rev. B **45**, 4536 (1992).
[5] N. Telang and S. Bandyopadhyay, Phys. Rev. B **48**, 18 002 (1993).
[6] N. Telang and S. Bandyopadhyay, Appl. Phys. Lett. **62**, 3161 (1993).
[7] N. Telang and S. Bandyopadhyay, Semicond. Sci. Technol. **9**, 955 (1994).
[8] N. Telang and S. Bandyopadhyay, Phys. Rev. Lett. **73**, 1683 (1994).
[9] N. Telang and S. Bandyopadhyay, Phys. Low-Dimens. Struct. **9/10**, 63 (1996).
[10] M. Masale and N. C. Constantinou, Phys. Rev. B **48**, 11 928 (1993).
[11] SeGi Yu, K. W. Kim, M. A. Stroscio, G. J. Iafrate, and A. Ballato, Phys. Rev. B **50**, 1733 (1994).
[12] N. Bannov, V. Aristov, V. Mitin, and M. A. Stroscio, Phys. Rev. B **51**, 9930 (1995).
[13] N. Nishiguchi, Y. Ando, and M. N. Wybourne, J. Phys.: Condens. Matter (to be published); N. Nishiguchi, Phys. Rev. B **52**, 5279 (1995).
[14] S. Chaudhuri and S. Bandyopadhyay, J. Appl. Phys. **71**, 3027 (1992).
[15] M. Büttiker, Phys. Rev. B **38**, 9375 (1988).
[16] W. M. Visscher, A. Migliori, T. M. Bell, and R. A. Reinert, J. Acoust. Soc. Am. **90**, 2154 (1991); A. Migliori, J. L. Sarrao, W. M. Visscher, T. M. Bell, M. Lei, Z. Fisk, and R. G. Leisure, Physica B **183**, 1 (1993).
[17] R. W. Morse, J. Acoust. Soc. Am. **20**, 833 (1948).
[18] R. W. Morse, J. Acoust. Soc. Am. **22**, 219 (1950).
[19] M. Lundstrom, in *Fundamentals of Carrier Transport*, edited by G. W. Neudeck and R. F. Pierret, Modular Series on Solid State Devices (Addison-Wesley, Reading, MA 1990), Vol X.
[20] K. V. Pederson, A. Savin, O. P. Hansen, and N. Ya. Minina (unpublished).
[21] Th. Englert, J. C. Mann, D. C. Tsui, and A. C. Gossard, Solid State Commun. **45**, 989 (1983).